Robust Single-Shot Fringe Pattern Projection for Three-dimensional Measurements

Budianto and Daniel P.K. Lun*
Centre for Signal Processing, EIE
Department of Electronic and Information Engineering
The Hong Kong Polytechnic University
Hong Kong
*enpklun@polyu.edu.hk

Weiping Zhu
Department of Electrical and Computer Engineering
Concordia University
Montreal, Canada
weiping@ece.concordia.ca

***Abstract*— Although single-shot fringe projection profilometry (FPP) techniques are known to allow effective 3-dimensional measurements (3D) of moving objects, their robustness is often of concern particularly if the object has vivid textures on its surface. Besides, traditional approaches only focus on 3D measurements but ignore the need in many applications of mapping the 3D measurements to the 2-dimensional (2D) textures of the object. In this paper, we present a novel single-shot FPP technique for measuring the 3D model of an object and at the same time estimating its 2D textures. The proposed technique employs a morphological component analysis (MCA) method to separate the fringe patterns and object textures from a fringe image. To further improve the efficiency in identifying the fringe pattern and object texture coefficients, a spatially adaptive thresholding method is developed for MCA. Experimental results show that the proposed technique can significantly improve the robustness of single-shot FPP techniques even when the object has vivid textures on its surface. Besides, it can simultaneously generate the 2D texture image of the object which can hardly be achieved by the traditional single-shot FPP approaches.**

Keywords—Fringe pattern projection, 3-dimensional measurement, morphological component analysis, wavelets

I. INTRODUCTION

Fringe projection profilometry (FPP) is an active range sensing technique which plays an important role in various disciplines that require 3-dimensional (3D) measurements, e.g., medical tomography [1], 3D scene reconstruction [2], industrial quality control [3], 3D face reconstruction [4], and 3D scanning for complex scenes [5]. A typical FPP system consists of a projector that projects a set of spatially periodic fringe patterns onto an object. A camera is then used to capture the deformed fringe patterns as shown on the object's surface. Since the amount of deformation actually encodes the 3D information of the object, various techniques have been developed to measure the deformation, and thus the 3D model of the object can be obtained.

However, FPP is restricted under the fundamental trade-off between the spatial accuracy and temporal accuracy. This fundamental trade-off has triggered the development of two classes of FPP methods: single-shot and multiple-shot FPP. For multiple-shot FPP methods, multiple frames of fringe pattern, each with certain amount of phase shifted, are projected on the target object. While multiple-shot FPP methods are usually more robust, they are not suitable to the applications where either the object or the measuring device cannot be kept static. Although some recent works have been proposed to minimize the motion error in multiple-shot FPP [6], their performance when applying to real life dynamic problems still have much room for further improvement.

In contrast, single-shot FPP methods require only projecting one fringe pattern to complete a 3D measurement. So it does not have the problem of the multiple-shot FPP as mention above. However, single-shot FPP methods always have low spatial accuracy and can be erroneous if the object's surface contains vivid textures, e.g., color patterns or strong reflection, etc. A number of approaches have been proposed to tackle this problem either by subtracting the captured fringe pattern with additional flat image (without pattern) [7], using complex wavelet to estimate bias [8], or interpolating the peak intensities of fringes [9]. However [7] requires additional image and [8] assumes that there is no discontinuity in the image and the image texture is simple. [9] has a high computation complexity for interpolating the peak intensities of fringes. They all have their own deficiencies in terms of cost-effectiveness and robustness.

In fact, most traditional single-shot and multiple-shot FPP methods just focus on obtaining the 3D measurements. In this paper, we present a novel single-shot FPP technique for measuring the 3D model of an object and at the same time estimating its 2D textures. Specifically, it employs a morphological component analysis (MCA) [10] to separate the fringe patterns and object textures from a fringe image. Note that in a typical FPP setup, the fringe image captured by the camera can be considered as the sum of the deformed fringe patterns and the textures of the object. Furthermore, they have very different morphological structures that perfectly fits into the framework of MCA, which allows them to be effectively separated. Then we can make use of the separated fringe patterns to complete the 3D measurements, and the 2D textures of the object can also be obtained at the same time. However, traditional MCA methods which use a uniform threshold in its iterative optimization process are inefficient to FPP problem (as will be shown in Section III). In this paper, we propose a spatially adaptive thresholding method, which makes use of a switching median filter to estimate the spatially adaptive threshold required. Experimental results show that the

proposed technique can significantly improve the robustness of single-shot FPP techniques even when the object has vivid textures on its surface. Besides, it can simultaneously generate the 2D texture image of the object which can hardly be achieved by the traditional single-shot FPP approaches. An overview of the proposed FPP framework is shown in Fig. 1. The key ingredient of our proposed FPP framework is the MCA which will be explained in more detail in Section III.

II. Color Encoded FPP with MCA

In this work, we employ the color encoded phase shifting profilometry (PSP) method [11]. Rather than projecting a number of fringe patterns with different phase shifts in sequence as the traditional multiple-sort FPP methods, these fringe patterns are each encoded by a distinct color (for instance, red, green or blue) and combined into a single frame to project to the object. Mathematically, each color channel of the captured fringe image Y^c can be expressed as follows:

$$Y^c = Y_1^c + b^c \cos\left(\phi - \frac{2n\pi}{3}\right), \tag{1}$$

where the subscript $c \in \{r, g, b\}$ refers to the color channel red, green, and blue; Y_1^c refers to the textures of the object corresponding to a particular color channel; and b^c is the amplitude of the fringes of the same color channel; and $n \in \{1,0,-1\}$. In (1), ϕ is the phase of the fringe patterns, which are modulated by the 3D structure of the object. Assume that the luminance of Y^r, Y^g, and Y^b are I_1, I_2, and I_3, respectively. Ideally, the phase information ϕ in (1) can be evaluated from I_1, I_2, and I_3 by,

$$\hat{\phi} = \arctan\left[\sqrt{3}\frac{I_1 - I_3}{2I_2 - I_1 - I_3}\right], \tag{2}$$

which is the so-called PSP method. Unfortunately, the color filtering process for obtaining Y^c can have all kinds of errors since the object textures Y_1^c can also have the same color as the fringes. There needs to be another more effective process to separate the fringe patterns and the object textures.

III. MCA USING ADAPTIVE THRESHOLD

Recall that the captured fringe image, Y containing the object textures and the color encoded fringe patterns. Hence it can be mathematically modeled as follows:

$$Y = Y_1 + Y_2, \tag{3}$$

where Y_1 is the object texture; and Y_2 is the sinusoidal fringe pattern, i.e., the second term on the right hand side of (1). Since the object textures and fringe patterns usually have very different morphological structures, it fits very well to the framework of MCA. We can use MCA to separate Y_1 and Y_2 from Y by solving the following constrained optimization problem,

$$\underset{Y1,Y2}{arg\,min} \|\omega_1\|_1 + \|\omega_2\|_1 + \lambda\left\|Y - \Phi_1\,\omega_1 - \Phi_1\,\omega_2\right\|_2, \tag{4}$$

where $\Phi_{i=1,2}$ are the dictionaries which generate the decomposition of $Y_{i=1,2}$ in $\Phi_{i=1,2}$: $Y_{i=1,2} = \Phi_{i=1,2}\omega_{i=1,2}$ and λ is the regularization parameter. Since many FPP applications require fast, if not real-time, performance, the implementation of $\Phi_{i=1,2}$ needs to have fast algorithms. Hence there are not too many choices but only the structured transforms can meet the requirement. Following the traditional MCA, we use the tunable Q-factor wavelet transform (TQWT) to implement Φ_1 since it can better take care of the discontinuities in the object textures. And for the dictionary of the sinusoidal fringe component, i.e. Φ_2, we choose discrete cosine transform (DCT) due to its good selectivity for sinusoidal signals.

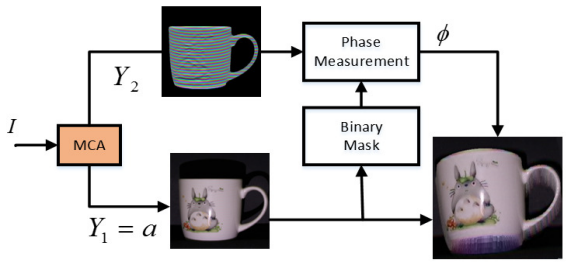

Fig. 1. FPP Framework using MCA

To solve the optimization problem in (4), MCA employs the iterative alternate thresholding algorithm. In this scheme, each term, i.e., ω_1 and ω_2, are updated alternately in each iteration. More specifically, at iteration kth, the estimation of $\hat{Y}_1^{(k)}$ and $\hat{Y}_2^{(k)}$ are obtained by hard thresholding, $\hat{Y}_{i=1,2}^{(k)} = \Pi_{\Phi_i,\lambda_i}(\hat{R}_i)$, where $\hat{R}_1^{(k)} = Y - \hat{Y}_2^{(k-1)}$ and $\hat{R}_2^{(k)} = Y - \hat{Y}_1^{(k-1)}$ are the residue obtained from the estimation of the previous iteration and the operator Π is defined as, $\Pi_{\Phi,\lambda}(\mathrm{X}) = \Phi\left(\delta_\lambda(\Phi^T X)\right)$, where δ_λ is a thresholding operator, i.e., hard thresholding. In conventional MCA algorithms, the initial threshold is commonly set automatically to the largest value, i.e., the maximum in magnitude of all coefficients ($\lambda_1 = \max(\|\Phi_1^T Y\|_\infty, \|\Phi_2^T Y\|_\infty)$, and it decreases linearly towards zero in each iteration [10]. Although it is simple, it is difficult to determine the number iteration to yield a successful separation. For fast decomposition with the least number of iteration, [12] employs an adaptive thresholding strategy by using the mean of maximum (MOM) approach, i.e. $\lambda_{i=1,2}^{(k)} = 0.5\left[\Phi_1^T r^{(k-1)} + \Phi_2^T r^{(k-1)}\right]$, where r is the residue from the previous iteration. However, the choice of uniform threshold is seldom verified with more complex data set such as fringe images, which is generally not exactly but only approximately sparse in the wavelet domain as illustrated in Fig. 2. As shown in the figure, the level 3 TQWT coefficients of the fringe component has strong magnitude (also appear as fringes) while it is not the case for those in level 5. Actually the coefficients at level 5 are similar for the images without fringes. The results of Fig. 2 show that the wavelet coefficients of the fringe component can also be very strong in some levels. A simple thresholding scheme cannot kill the fringe coefficient while keeping those for the object textures.

A. *Spatially Adaptive Threshold for Φ_1*

While it is not easy to find other dictionaries that can fulfill all the requirements as mentioned above, we continue to use TQWT in the proposed algorithm for the implementation of

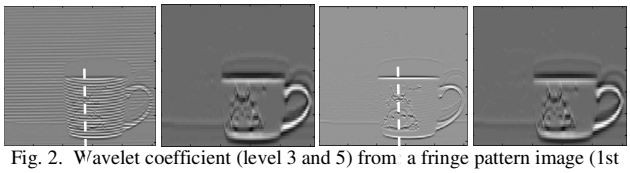

Fig. 2. Wavelet coefficient (level 3 and 5) from a fringe pattern image (1st two columns) and a flat image (the last two columns)

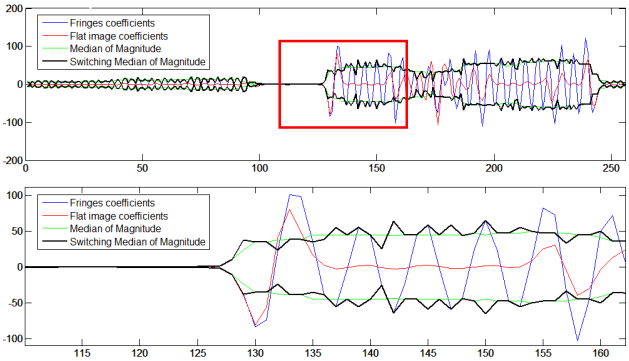

Fig. 3. The TQWT coefficient plots of the two dash lines in Fig. 2 (1st row) and its zoom version of red box (2nd row) respectively

Φ_1; but we suggest to develop a new spatially adaptive thresholding strategy in order to separate the fringe pattern and object textures efficiently in Φ_1. To illustrate the new thresholding scheme, let us have a closer look of the TQWT coefficients of the fringe image. We show in Fig. 3 an example of the TQWT coefficients taken from the dash lines in Fig. 2. In the figure, the blue lines are the TQWT coefficients of the fringe image which contains both the fringe component and texture component (the dash line of the 1st image in Fig. 2). The red lines show the TQWT coefficients of the texture component without fringes (the dash line of the 3rd image in Fig. 2). It can be seen that most parts of the blue lines are rather an oscillating signal with occasional jumps in magnitude. The jumps actually follow closely with the red lines, which are relatively are sparse. The jumps in magnitude actually correspond to the edges and sharp changes of the object textures. There are a few observations in Fig. 3 that guide us to develop a good threshold in Φ_1 for MCA. First, since our objective in Φ_1 is to kill the fringe coefficients (the oscillating coefficients between the jumps) while keeping those for the object textures (the jumps), the threshold should be set above the magnitude of the fringe coefficients but below the magnitudes of the textures coefficients. If it can be achieved, then all coefficients with magnitude smaller than the threshold can be removed (hard thresholding). Second, the magnitudes of the fringe coefficients can be different at different spatial locations. A global uniform threshold used in the traditional MCA algorithms is thus not appropriate in this problem. We need a spatially adaptive threshold.

To design a spatially adaptive threshold, intuitively we can apply a median filter with a suitable window to the coefficients such that all the jumps are smoothed out. The result is shown by the green line in the plot of Fig. 3. So all coefficients with magnitude below the green line will be removed. However, such strategy does not necessarily remove all fringe coefficients. As shown in the zoom-in box of Fig. 3, the median values (green line) are slightly below than the magnitude of the fringe coefficients. It allows some parts of fringe coefficients to be kept after thresholding.

To solve the problem, we propose in this paper a hard switching median filter scheme. The basic principle is that the median filtering used for generating the thresholds will only be applied to those wavelet coefficients where significant jumps are found. The rest of the coefficients will have the thresholds the same as their magnitudes. The result is shown by the black line in Fig. 3. It can be seen that the black line in general follows the blue line. But when the blue line has significant jumps in magnitude, the black line will be set lower than the blue line such that all coefficients of the jumps will be kept. The black line becomes the spatially adaptive threshold we needed.

The above strategy can be implemented as follows. Recall that $\omega_1(i,j)$ is the TQWT coefficient of the fringe image at spatial position (i,j). Let us denote $\lambda_1(i,j)$ as the threshold value in Φ_1 at (i,j); and $m^{i,j} = median\left(W^{ij}(|\omega_1|)\right)$ be the median filtering results of the magnitude of a set of ω_1 within a window W centered at (i,j). More specifically, we suggest the following switching median filtering scheme to determine the threshold,

$$\lambda_1(i,j) = \begin{cases} m^{i,j}, & \left|\left|\omega_1(i,j)\right| - m^{i,j}\right| \geq T \\ \left|\omega_1(i,j)\right|, & otherwise. \end{cases} \quad (5)$$

If $\left|\left|\omega_1(i,j)\right| - m^{i,j}\right|$ is greater than the threshold T, it is likely that $\left|\omega_1(i,j)\right|$ corresponds to the jumps in the coefficients. So the threshold at (i,j) should be set as $m^{i,j}$. Otherwise, the threshold should be set as $\left|\omega_1(i,j)\right|$. Note that when $T = 0$, the switching scheme become a conventional median filter. In practice, both T and W are chosen according to the number of pixels for each period of the fringes. It can be determined during the calibration process. Note that their choices are not sensitive to the final result.

B. *Uniform Threshold for Φ_2*

Similar to the traditional MCA, we use a uniform threshold in Φ_2. However, a modification is made to allow the threshold to be more effective in FPP applications. At a particular k iteration during the MCA process, let us first assume that $\bar{\omega}_{i=1,2}^{(k-1)} = \omega_{i=1,2} - \hat{\omega}_{i=1,2}^{(k-1)}$, where $\hat{\omega}_2^{(k-1)}$ is the coefficients that have been found in the previous iteration and $\bar{\omega}_2$ is the estimation error of Φ_2 in the coefficient domain. It is known from [12] that λ_2 has to be chosen as, $\left\|\Phi_2^{\mathrm{T}}\Phi_1\bar{\omega}_1^{(k-1)}\right\|_\infty < \lambda_2 < \left\|\bar{\omega}_2^{(k-1)}\right\|_\infty$. It can be interpreted that a good threshold must be lower than the estimation error of the texture component in Φ_2, but larger than the estimation error of the fringe component in Φ_2. In practice, these lower and upper bounds cannot be computed because we never have any knowledge about the estimation error. Hence, [12] estimates the threshold value by finding the mean of

maximum value of the total residual $r^{(k)} = Y - \hat{Y}_1^{(k-1)} - \hat{Y}_2^{(k-1)}$ in the domain Φ_1 and Φ_2. Unlike [12], we can determine the upper bound of λ_2 using the maximum of λ_1. It is because the thresholded coefficients of the fringe by λ_1 will be sparser in Φ_2 domain. More specifically, as mentioned previously in Φ_1, the nearly constant coefficients are in fact the fringe component which are sparser in Φ_2 and thus they are represented by some non-zero elements larger than λ_1. This entails with high probability that, $\|\Phi_2 r^{(k)}\|_\infty < \lambda_2 < \|\lambda_1\|_\infty$. In this scheme, $\lambda_2^{(k)}$ is defined as,

$$\lambda_2 = 0.5\left(\|\Phi_2 r^{(k)}\|_\infty + \|\lambda_{ij}\|_\infty\right). \quad (6)$$

Based on the proposed thresholding strategies in Section IIIA and IIIB, the new iterative alternate thresholding algorithm is summarized as follows:

1. Initialize $Y = Y^c, Y_1^{(0)} = 0, Y_2^{(0)} = 0$
2. Repeat until $\lambda_2 < \lambda_{min}$
   a. Compute the residual $r_1^{(k)}$, $r_1^{(k)} = Y - \hat{Y}_2^{(k-1)}$
   b. Compute the transform coefficient $\omega^{(k)} = \Phi_1^T r_1^{(k)}$.
   c. Estimate threshold λ_1 by (5)
   d. Compute $\hat{Y}_1^{(k)}$, $\hat{Y}_1^{(k)} = \Phi_1\left(\delta_{\lambda_{ij}}(\omega^{(k)})\right)$
   e. Compute the residual term $r_2^{(k)}$, $r_2^{(k)} = Y - \hat{Y}_1^{(k)}$
   f. Estimate threshold λ_2 by (6)
   g. Compute $\hat{Y}_2^{(k)}$ by hard thresholding $\hat{Y}_2^{(k)} = \Phi_2\left(\delta_{\lambda^{(k)}}(\Phi_2^T r_2^k)\right)$
   h. Compute the total residual $r = Y - \hat{Y}_1^{(k)} - \hat{Y}_2^{(k)}$

λ_{min} is set to be zero or a few times from the noise standard deviation when noise is contained in the data.

IV. Experimental Results and Comparison

A series of experiments were performed to evaluate the accuracy the proposal single-shot FPP technique. The first experiment was performed by applying the proposed technique to a flat board whose dimension is 45cm × 35cm. It serves as an objective comparison of the accuracy of different methods for separating the fringe pattern and the object textures. In this experiment, we compare the proposed approach with the conventional color encoded PSP (CPSP), the conventional MCA with CPSP (CPSP-MCA) as well as the bias removal strategy [8] with CPSP (CPSP-BR) (CPSP-BR). All methods employ a simple Goldstein phase unwrapping algorithm [13] to construct the 3D model of the object from the measured phase angle. As a general practice, a small marker is placed at the center of the fringe image for calibration. In this experiment, a color encoded fringe pattern is projected unto a flat board and a camera captures the reflected image for 50 times. The total number of reconstruction point is 1,008,016 by ignoring a few pixels in the boundary which contain some artifacts. The reconstruction phase error in terms of root mean squares (RMS) is then calculated by averaging the whole surface.

Fig. 4 shows the comparison result of the conventional CPSP, CPSP-MCA, CPSP-BR and the proposed method.

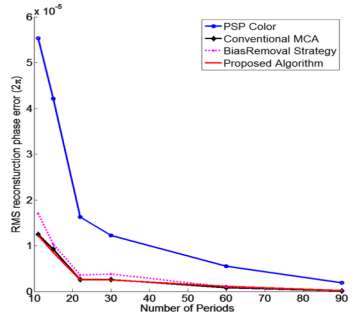

(a)

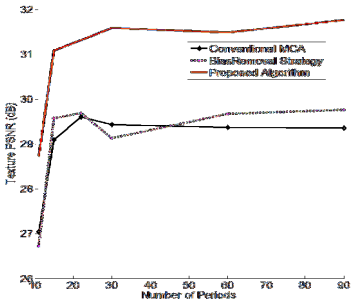

(b)

Fig. 4. A comparison of the experimental results of CPSP, CPSP-MCA, CPSP-BR, and the proposed method in 3D measurements (a); and in retrieving the object textures (b).

Fig. 5. Texture images obtained using different approaches. (1st column) results of CPSP-MCA; (2nd column) results of CPSP-BR; (3rd column) results of the proposed approach; (4th column) the ground truth.

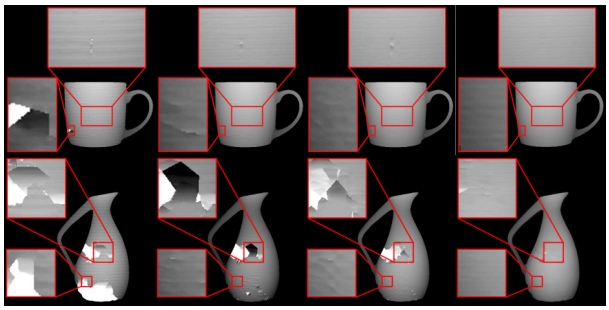

Fig. 6. The measured 3D models of a cup with some texture (top row) and a jar with vivid texture (bottom row) using different approaches: (1st column) CPSP; (2nd column) CPSP-MCA; (3rd column) the CPSP-BR; (4th column) the proposed technique.

Since the results for using different number of fringe periods in the projection patterns can be different, we plot the results in terms of the number of periods. As shown in Fig. 4(a), CPSP has the lowest accuracy in 3D measurements. And since it cannot recover the object textures, there is no result for CPSP in Fig. 4(b). Comparing with CPSP-MCA and CPSP-BR, it is apparent that the proposed technique can improve the accuracy in 3D measurements and also retrieve the object textures with good quality. As shown in the figure, the texture images retrieved by CPSP-MCA and CPSP-BR are bounded at about 26 to 28 dB PSNR (red line) respectively, while the proposed technique can give a PSNR up to 30 dB.

To understand the actual performance of the proposed technique, we implemented the proposed technique with a real FPP hardware setup. It consists of a digital light processing (DLP) projector having a 2000:1 contrast ratio and a digital camera having a 22.2 x 14.8mm CMOS sensor and a 17-50mm lens. Both devices are placed 700mm – 1200mm from the target object. As shown in Fig. 5 and Fig. 6, we considered two scenes in the experiments: (a) a cup with some textures on its surface; and (b) a jar with vivid textures. The results of the comparison are depicted in Fig. 5 and Fig. 6. The ground truth is generated by projecting the scenes using 50 fringes patterns and adopting the color encoded PSP for 3D measurements. As seen in Fig. 6, the resulting 3D models generated by CPSP are erroneous for objects with textured surface due to the color crosstalk and bias of the object textures. Meanwhile CPSP-MCA, CPSP-BR and the proposed method carry out extra measures to reduce the interference due to the object textures. They enhance the imperfect fringe patterns to allow better 3D measurements. But clearly, the proposed technique performs better than all other comparing approaches (the third column in Fig. 6) due to the enhanced MCA method.

Fig. 5 shows the results of object texture retrieval. Although the conventional MCA can separate the fringes and object textures, the resulting object texture images are rather blur as shown in Fig. 5 (1st column). It is due to the ineffective uniform threshold used in each iteration which cannot kill the fringe coefficients in Φ_1 effectively. The same is applied to the CPSP-BR method (2^{nd} column of Fig. 6). On the contrary, the proposed method gives more accurate spatially adaptive thresholds. They allow a good separation of the fringes and object textures; and leads to the good results as shown in Fig. 5 (3rd column).

V. CONCLUSION

In this research, we proposed a robust single-shot fringe projection profilometry (FPP) technique that effectively measures the 3D model of an object while at the same time captures its texture image. This FPP employs a conventional color encoded phase shifting profilometry (PSP) method such that only a single color fringe pattern is projected. The key ingredient of the proposed technique is an improve morphological component analysis (MCA) algorithm for separating the fringe patterns and object textures. In this algorithm, a switching median filter is employed to tune the optimum threshold. This thresholding strategy differs from the traditional ones in that it is accurate, adaptive, and contextual. Besides, it does not require a good initialization to guarantee the convergence of the iteration. Experimental results have demonstrated the effectiveness of the proposed technique for measuring the 3D model of different objects while their texture images can also be retrieved at the same time without additional hardware or fringe pattern projections. We believe that it will open a new research direction for single-shot FPP by which the simultaneous depth and image sensing devices can be realized.

ACKNOWLEDGMENT

The research work described in this paper is fully supported by the Hong Kong Research Grant Council under research grant PolyU 5210/13E.

REFERENCES

[1] B. Shi, B. Zhang, F. Liu, J. Luo, and J. Bai, "360° Fourier Transform Profilometry in Surface Reconstruction for Fluorescence Molecular Tomography," *IEEE J. Biomed. Health Inform.,* vol. 17, pp. 681-689, 2013.

[2] R. R. Garcia and A. Zakhor, "Consistent Stereo-Assisted Absolute Phase Unwrapping Methods for Structured Light Systems," *IEEE J. Sel. Topics Signal Process.,* vol. 6, pp. 411-424, 2012.

[3] Z. Song, R. Chung, and X.-T. Zhang, "An Accurate and Robust Strip-Edge-Based Structured Light Means for Shiny Surface Micromeasurement in 3-D," *IEEE Trans. Ind. Electron.,* vol. 60, pp. 1023-1032, 2013.

[4] S. Zhang, "High-resolution, High-speed 3-D Dynamically Deformable Shape Measurement Using Digital Fringe Projection Techniques," in *Advances in Measurement Systems*, M. K. Sharma, Ed., ed: InTech, 2010, pp. 29-50.

[5] Budianto and D. P. K. Lun, "Robust Fringe Projection Profilometry via Sparse Representation," *IEEE Trans. Image Process.,* vol. 25, pp. 1726-1739, 2016.

[6] P. Cong, Z. Xiong, Y. Zhang, S. Zhao, and F. Wu, "Accurate Dynamic 3D Sensing With Fourier-Assisted Phase Shifting," *IEEE J. Sel. Topics Signal Process.,* vol. 9, pp. 396-408, 2015.

[7] H. Guo and P. S. Huang, "3-D shape measurement by use of a modified Fourier transform method," in *Proc. SPIE 7066, Two- and Three-Dimensional Methods for Inspection and Metrology VI*, 2008, pp. 70660E-70660E-8.

[8] W. W.-L. Ng and D. P.-K. Lun, "Effective bias removal for fringe projection profilometry using the dual-tree complex wavelet transform," *Appl. Opt.,* vol. 51, pp. 5909-5916, 2012.

[9] H. Hyowon, P. Jaesik, and K. In So, "Dense Depth and Albedo from a Single-Shot Structured Light," in *Proc. Int. Conf. 3D Vision (3DV)*, 2015, pp. 127-134.

[10] J. L. Starck, Y. Moudden, J. Bobin, M. Elad, and D. L. Donoho, "Morphological component analysis," 2005, pp. 59140Q-59140Q-15.

[11] C. Je, S. W. Lee, and R.-H. Park, "Color-Phase Analysis for Sinusoidal Structured Light in Rapid Range Imaging," in *Proc. 6th Asian Conf. on Computer Vision*, 2004.

[12] J. Bobin, J. L. Starck, J. M. Fadili, Y. Moudden, and D. L. Donoho, "Morphological Component Analysis: An Adaptive Thresholding Strategy," *IEEE Trans. Image Process.,* vol. 16, pp. 2675-2681, 2007.

[13] R. M. Goldstein, H. A. Zebker, and C. L. Werner, "Satellite radar interferometry: Two-dimensional phase unwrapping," *Radio Science,* vol. 23, pp. 713-720, 1988.